Supplementary Figures and Table

Enhanced Potassium-ion Storage of the 3D Carbon Superstructure by Manipulating the N Species and Morphology via Bottom-up Synthesis Method

Yanhua Li[1, 2], Kui Xiao[2], Cong Huang[1], Jin Wang[3], Ming Gao[1], Aiping Hu[1], Qunli Tang[1], Binbin Fan[1], Yali Xu[1], Xiaohua Chen[1, *]

[1]College of Materials Science and Engineering, Hunan University, Changsha 410082, China.

[2]College of Materials and Chemistry Engineering, Hunan Institute of Technology, Hengyang 421002, China.

[3]Zhuzhou Times New Material Technology Co., LTD, Zhuzhou 412007, China.

* Xiaohua Chen, E-mail: xiaohuachen@hnu.edu.cn

Content

Note 1 Photograph of monomer salts

Fig. S1. Photograph of monomer salts

Note 2 Photograph of PI particles

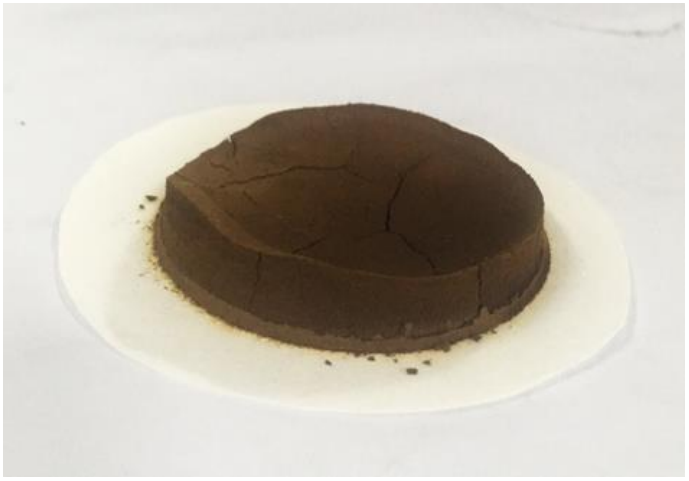

Fig. S2. Photograph of PIs.

Note 3 FT-IR and TGA analysis

FT-IR spectra were recorded on a Bruker Tensor 27. Resolution was set to 2-4 cm^{-1}, and spectra were recorded from 4000 to 600 cm^{-1}.

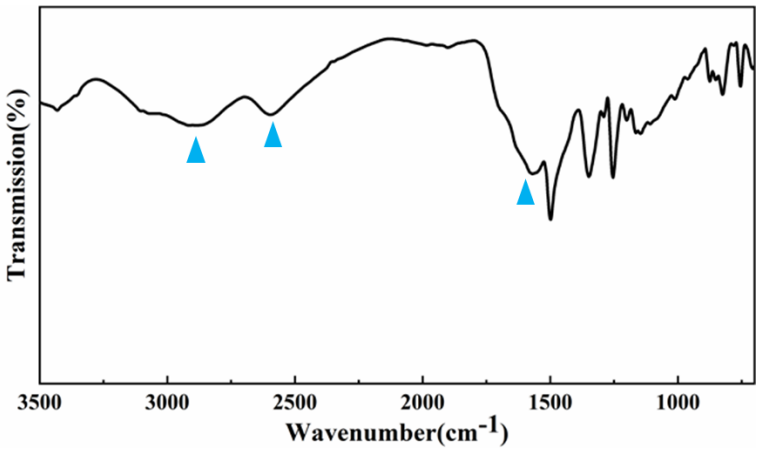

Fig. S3. FT-IR spectra of monomer salt [$ODA^{2+}PMDA^{2-}$]. ▲: typical monomer salt modes, $\tilde{\nu}_{as}$ (Ar-NH^{3+}) ≈ 2840 cm^{-1}, $\tilde{\nu}_s$ (Ar-NH^{3+}) ≈ 2580 cm^{-1}, $\tilde{\nu}_s$(C=O, Ar-COO-) ≈ 1570 cm^{-1}.

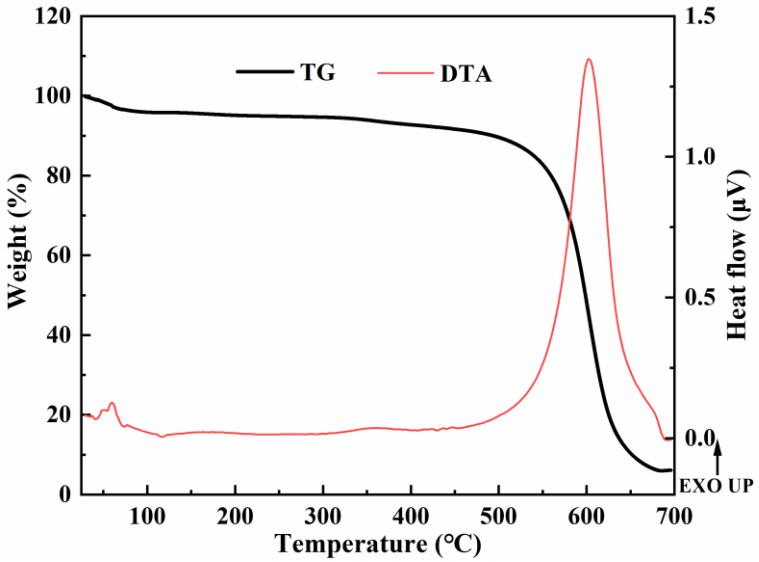

Fig. S4. TGA curve of PI-5 tested in N_2 atmosphere.

Note 4 SEM images

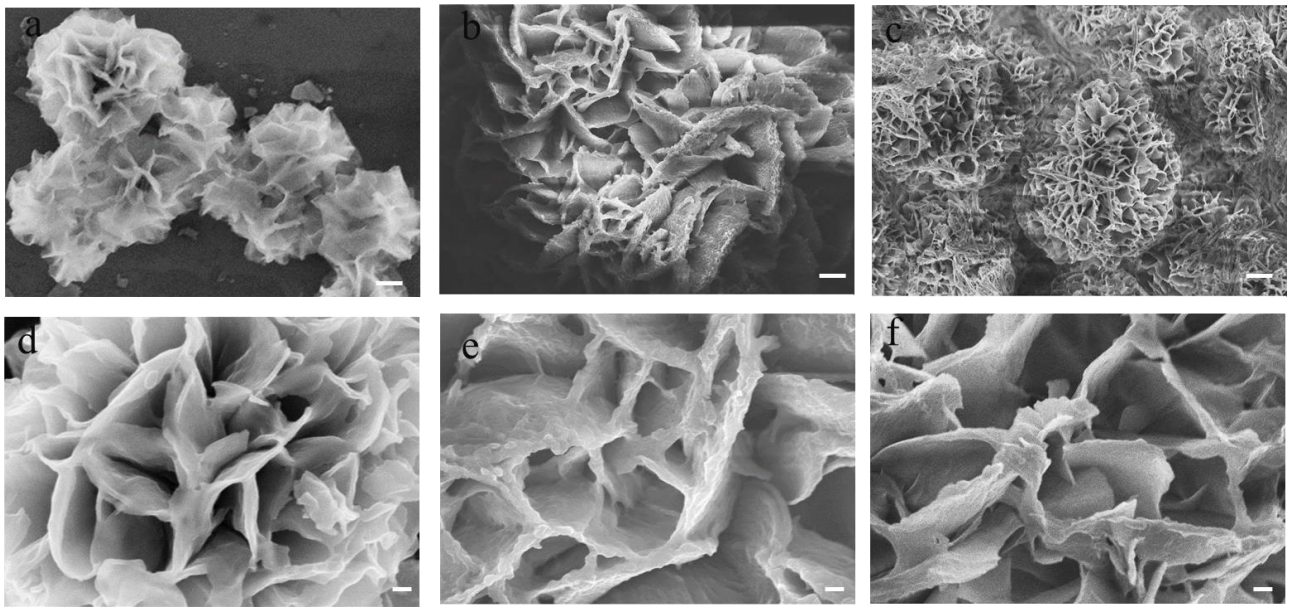

Fig. S5. SEM images of (a) PI-1, (b) PI-2, (c) PI-4, (d) NCS-1, (e) NCS-2, (f) NCS-4. Scale bar: (a)-(c) 2 μm, (d)-(e) 200 nm.

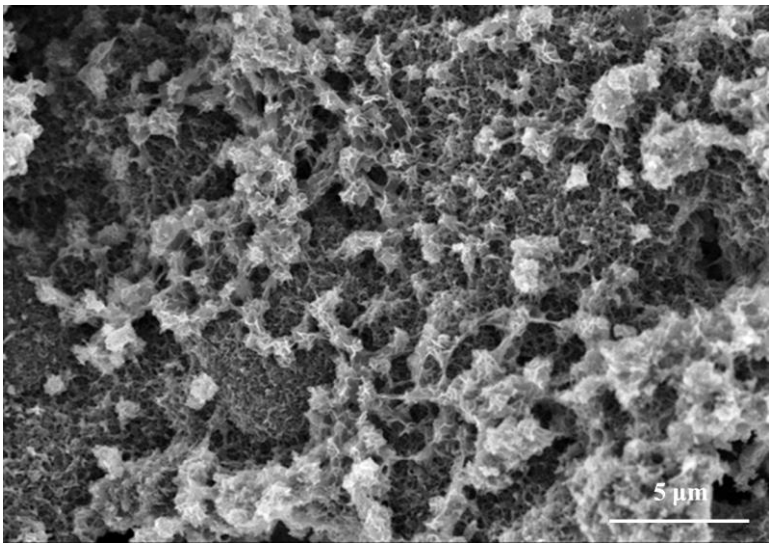

Fig. S6. SEM images of PI-6

Note 5 Nitrogen adsorption-desorption isotherms of NCSs

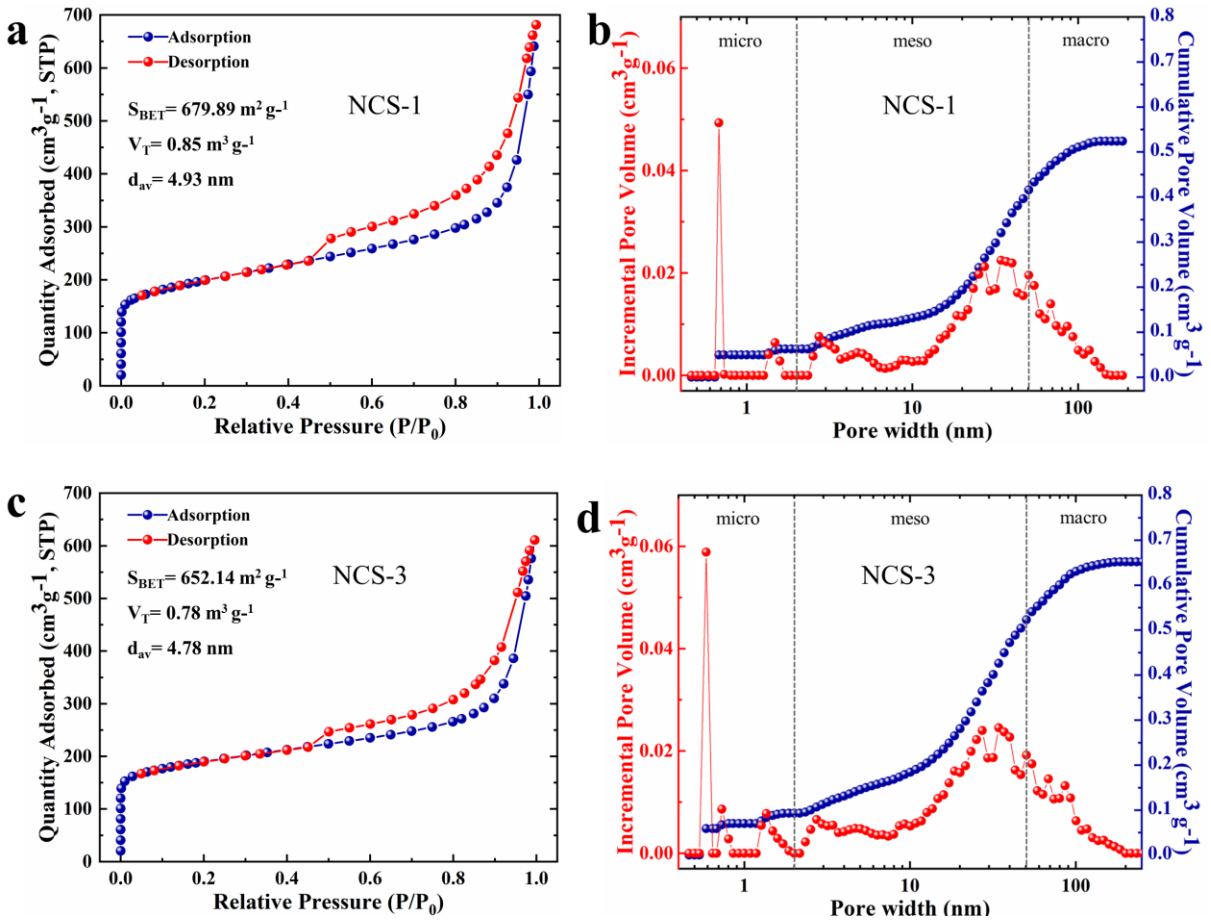

Fig. S7. a) Nitrogen adsorption-desorption isotherms of the NCS-1. b) Pore size distribution of the NCS-1. c) Nitrogen adsorption-desorption isotherms of the NCS-3. d) Pore size distribution of the NCS-3.

Note 6 XPS and high-resolution XPS spectra of NCSs

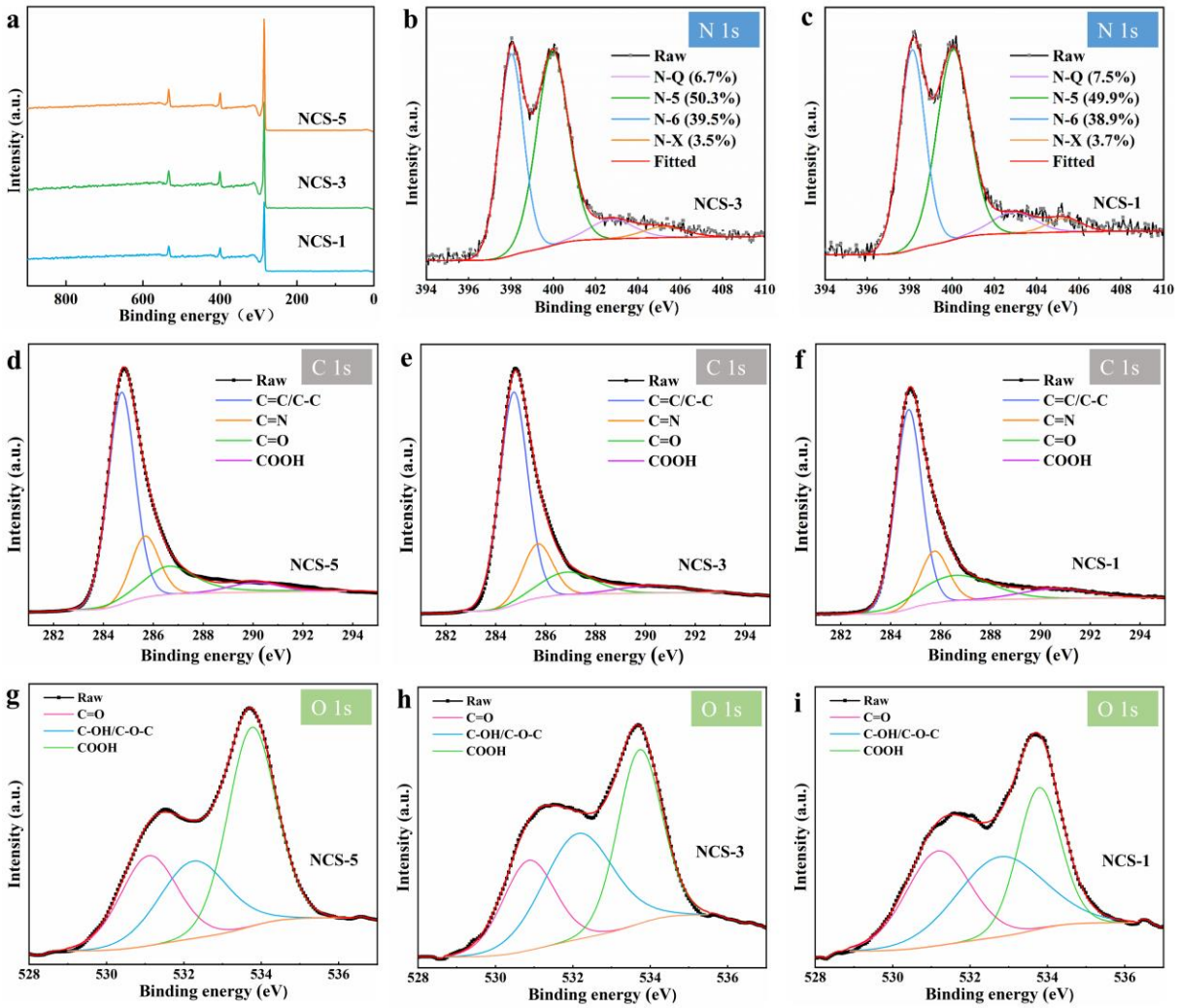

Fig. S8. XPS survey spectra. a) Survey spectrum of XPS of NCSs. N 1s high-resolution XPS spectra of NCSs: b) NCS-3, c) NCS-1. C 1s high-resolution XPS spectra of NCSs: d) NCS-5, e) NCS-3, d) NCS-1. O 1s high-resolution XPS spectra of NCSs: g) NCS-5, h) NCS-3, e) NCS-1.

Note 7 Characteristics of NCSs

Table S1 Content of element by EA and N-doped type by XPS

Sample	C (%)	N (%)	H (%)	O (%)	N type (%)			
					N-5	N-6	N-X	N-Q
NCS-5	76.18	9.12	3.22	11.48	52.0	40.7	1.1	6.2
NCS-3	76.59	8.88	3.68	10.85	50.6	39.2	3.5	6.7
NCS-1	76.89	8.45	3.91	10.75	50.1	38.9	3.7	7.5

Fig. S9 presents the FTIR spectrum of PI and NCSs. The bands of PI at 1780, 1720 cm^{-1} are attributed to the stretching and bending vibration of C=O, the peak at 1381 cm^{-1} belongs to the stretching vibration of C-N-C. The other peaks of PI at 1502 and 1248 cm^{-1} are assigned to the C-C stretching of benzene ring and the C-O-C stretching, respectively [1]. Due to the high thermal stability of PI, the weak characteristic peak of the C=O and C-H bond remained in the NCSs after 600 ℃ pyrolysis, as shown in the FTIR spectrum. The emerging peaks of NCSs at 1500–1610 cm^{-1} and 1000–1320 cm^{-1} are assigned to the stretching vibration of the C=C bond and C-N bond derived from the pyrolysis [2]. FTIR results indicate the high oxygen-containing and nitrogen-containing groups of NCSs, which is in accordance with the high O content from EA result and lowest graphitization degree from Raman analysis (I_D/I_G=2.9).

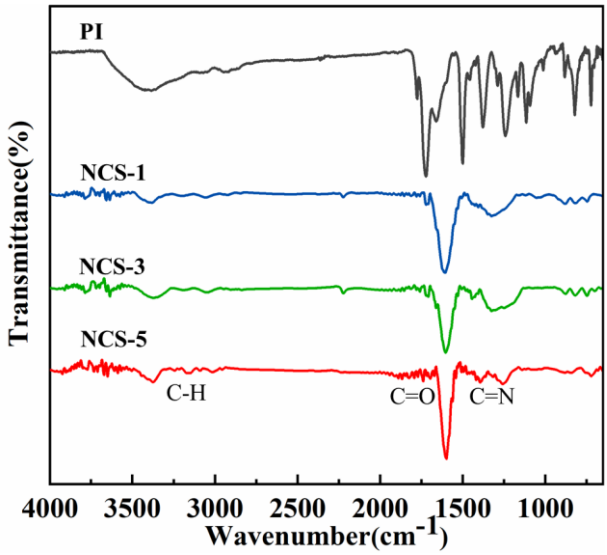

Fig. S9. FI-IR spectrum of PI and NCSs

Note 8 Electrochemical performance of NCSs as PIB anodes.

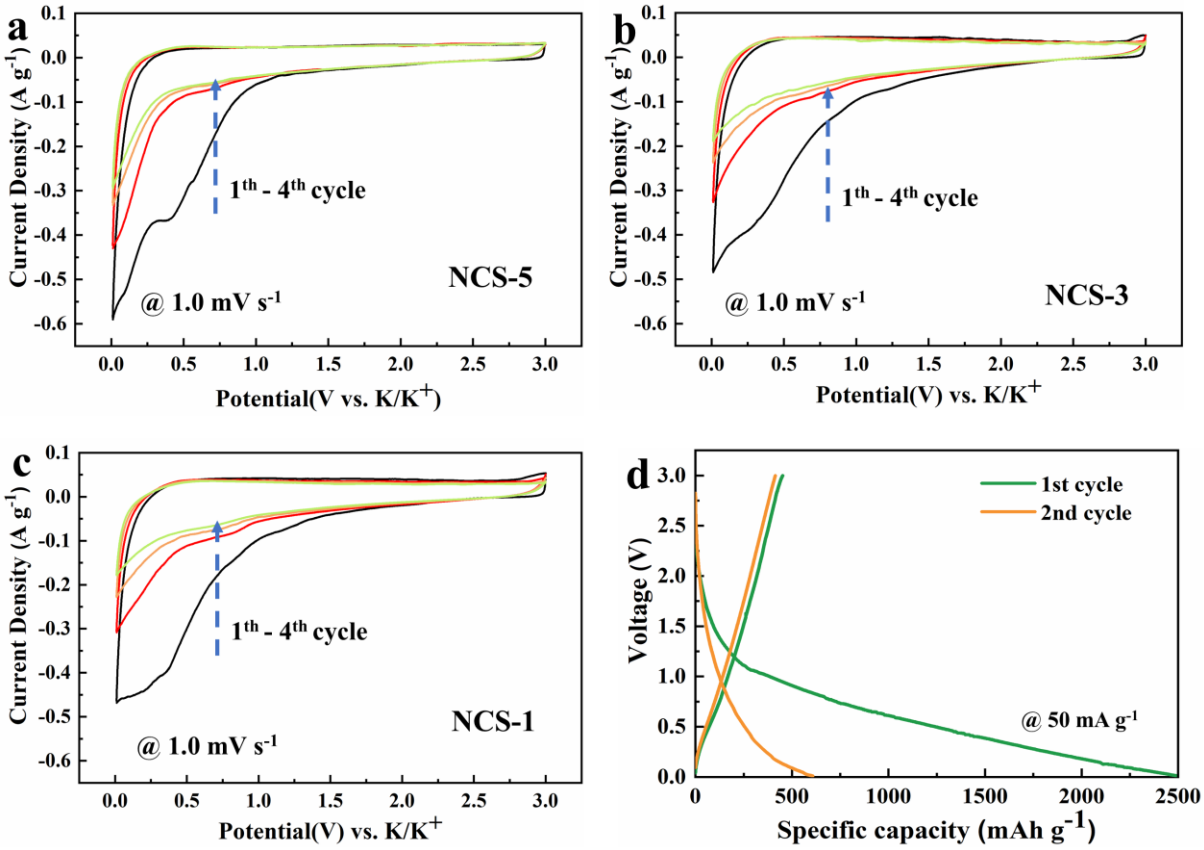

Fig. S10. Electrochemical performance of NCSs as PIB anodes in half cells. a-c) Cyclic voltammetry (CV) of the NCSs electrode for PIBs between 0.01 V and 3.0 V with a scan rate of 0.1 mV/s. d) Potassiation and depotassiation profiles of the NCS-5 electrode for the first cycle at 50 mA g^{-1}.

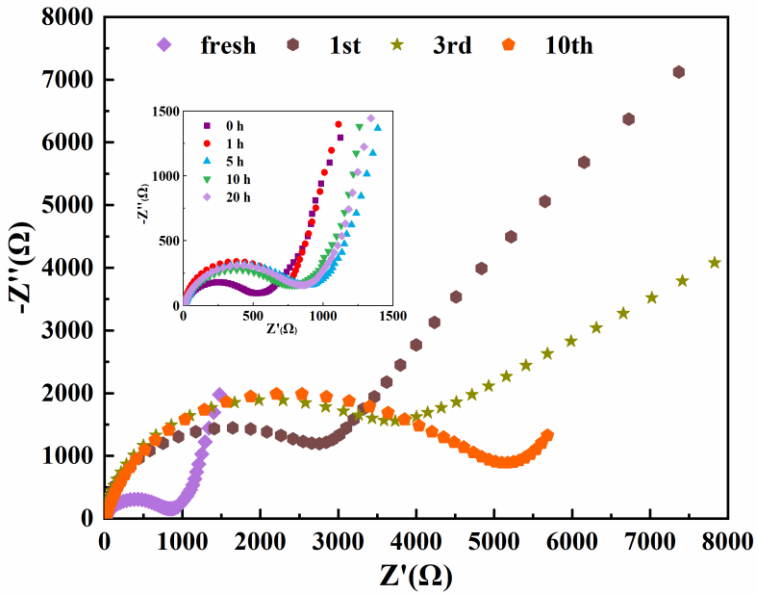

Fig. S11 EIS analysis of NCS-5.

Table S2 Comparison of the potassium-ion storage performances of the NCS-5 anode and carbon anodes published in the relative literatures.

Materials	**Sample labels**	**ICE (%) @ 50 mA g^{-1}**	**Reversible capacities mA h g^{-1} @ mA g^{-1}**	**Cyclability (capacity retention) mA h g^{-1} @ mA g^{-1}@ cycle number**	**Refs**
N doped 3D carbon superstructure	NCS-5	27.8	302 @ 50	205 @ 1000 @ 2000	This work
graphitic carbon nanocage	CNC	40 @ 0.2 C	195 @ 0.2 C	-	[3]
hard–soft composite carbon	HCS-SC	67 @ 0.1 C	230 @ 0.5 C	200 @ 1C @ 200	[4]
N/O dual-doped hard Carbon	NOHPHC	25	365 @ 25	118 @ 3000 @ 4000	[5]
N doped carbon nanofibers	NCNF-650	49	248 @ 25	146 @ 2000 @ 4000	[6]
N/O dual-doped carbon network	NOCN	47	464.9 @ 50	160 @ 5000 @ 4000	[7]
D-doped hierarchical porous carbon	N-HPC	-	292 @ 100	157 @2000@ 12000	[8]
S-doped RGO sponges	S-RGO-600	65	361 @ 50	229 @1000 @500	[9]
S/O codoped hard carbon	PCMs	61.7	226.6 @ 50	108.4 @ 1000 @ 2000	[10]
Phosphorus and oxygen dual-doped graphene	PODG	22.6	474 @ 50	160 @ 2000 @ 600	[11]
few-layer F-doped graphene foam	FFGF	41.2	326.1 @ 50	165.9 @ 500 @ 200	[12]
Phosphorus doped N-rich honeycomb-like carbon	PNHC	56.9	419.3 @ 100	270.4 @ 1000 @ 2000	[13]
free-standing nitrogen-doped carbon nanotube	NCSCNT	14.2	323 @ 20	236 @ 20 @100	[14]

RGO: reduced graphene oxide; ICE: initial Coulombic efficiency.

"-" stands for unknown value.

1 C = 279 mA g^{-1}

Note 9 Formation energies calculation of the three N-doped carbon via DFT

Calculations were based on the density functional theory (DFT) using the generalized gradient approximation [15] for the exchange–correlation potential prescribed by Perdew–Burke–Ernzerhof, which was implemented in DMol^3 package [16]. Allelectron calculations were employed with the double numerical basis sets plus polarization functional (DNP). A supercell (5×5) with the periodic boundary conditions on the x–y plane was employed. The vacuum space was set with 20 Å in the z direction to avoid the interactions between periodic images. Parameter settings wee set by the previously reported method with the optimization results [17].

The formation energies of vacancy graphene and vacancy doped-graphene was calculated according to the following definition:

$$\Delta E_1 = E_{vacancy} - E_{pure} + E_C \qquad (1)$$

$$\Delta E_2 = E_{doped} - E_{vacancy} - E_N + E_C \qquad (2)$$

$$\Delta E_3 = E_{doped} - E_{pure} - E_N + E_C \qquad (3)$$

where $E_{vacancy}$ is the total energy of the vacancy graphene, E_{doped} is the total energy of the doped graphene, E_{pure} is the total energy of the pure graphene, and E_C is the total energy from C atom calculated from the corresponding pure/vacancy graphene, E_N was obtained from N in the gas phase (N_2 molecule). All these energies are always taken from simulations using the same basis set.

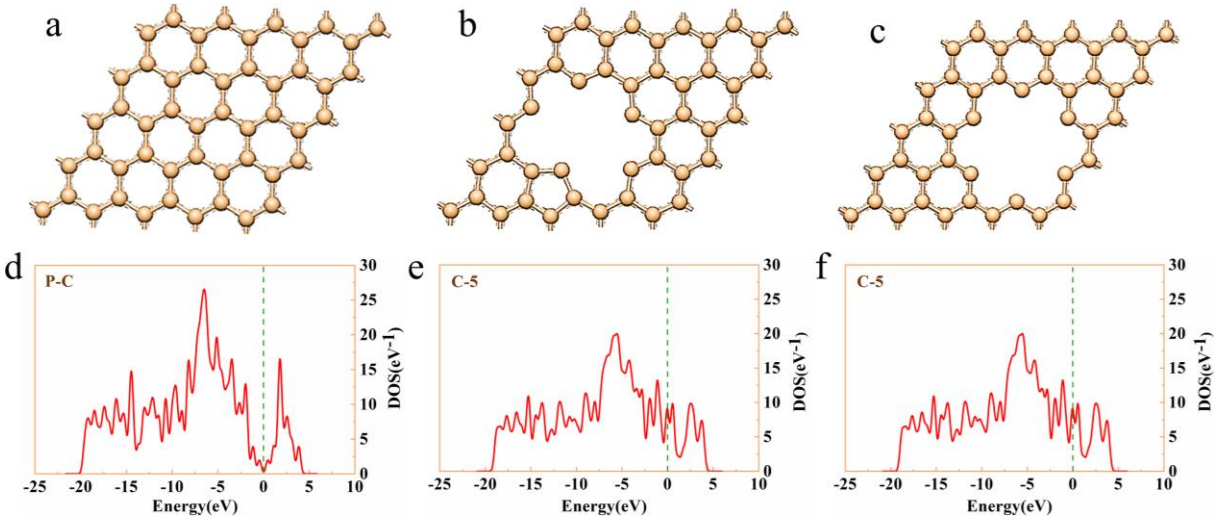

Fig. S12. Top views of the configurations of pure graphene P-C (a), vacancy graphene for C-5 (b), and vacancy graphene for C-6 (c). The density of states (DOS) for pristine C (d), vacancy graphene for C-5 (e), and vacancy graphene for C-6 (f).

Supplementary References

1. S. Zeng, L. Guo, F. Cui, Z. Gao, J. Zhou, J. Shi. Template-free synthesis of crystalline polyimide spheres with radiate branches. Mater Lett. **64**(5), 625-627 (2010). https://doi.org/10.1016/j.matlet.2009.12.024
2. Q. Wu, J. Liu, C. Yuan, Q. Li, H.-g. Wang. Nitrogen-doped 3d flower-like carbon materials derived from polyimide as high-performance anode materials for lithium-ion batteries. Appl Surf Sci. **425**, 1082-1088 (2017). https://doi.org/10.1016/j.apsusc.2017.07.118
3. B. Cao, Q. Zhang, H. Liu, B. Xu, S. Zhang, T. Zhou, J. Mao, W. K. Pang, Z. Guo, A. Li, J. Zhou, X. Chen, H. Song. Graphitic carbon nanocage as a stable and high power anode for potassium-ion batteries. Advanced Energy Materials. **8**(25), 1801149 (2018). https://doi.org/10.1002/aenm.201801149
4. Z. Jian, S. Hwang, Z. Li, A. S. Hernandez, X. Wang, Z. Xing, D. Su, X. Ji. Hard–soft composite carbon as a long-cycling and high-rate anode for potassium-ion batteries. Adv Funct Mater. **27**(26), 1700324 (2017). https://doi.org/10.1002/adfm.201700324
5. J. Yang, Z. Ju, Y. Jiang, Z. Xing, B. Xi, J. Feng, S. Xiong. Enhanced capacity and rate capability of nitrogen/oxygen dual-doped hard carbon in capacitive potassium-ion storage. Adv Mater. **30**(4), 1700104 (2018). https://doi.org/10.1002/adma.201700104
6. Y. Xu, C. Zhang, M. Zhou, Q. Fu, C. Zhao, M. Wu, Y. Lei. Highly nitrogen doped carbon nanofibers with superior rate capability and cyclability for potassium ion batteries. Nature Communications. **9**(1), 1720 (2018). https://doi.org/10.1038/s41467-018-04190-z
7. J. Ruan, Y. Zhao, S. Luo, T. Yuan, J. Yang, D. Sun, S. Zheng. Fast and stable potassium-ion storage achieved by in situ molecular self-assembling n/o dual-doped carbon network. Energy Storage Materials. **23**, 46-54 (2019). https://doi.org/10.1016/j.ensm.2019.05.037
8. X. Zhou, L. Chen, W. Zhang, J. Wang, Z. Liu, S. Zeng, R. Xu, Y. Wu, S. Ye, Y. Feng, X. Cheng, Z. Peng, X. Li, Y. Yu. Three-dimensional ordered macroporous metal–organic framework single crystal-derived nitrogen-doped hierarchical porous carbon for high-performance potassium-ion batteries. Nano Lett. **19**(8), 4965-4973 (2019). https://doi.org/10.1021/acs.nanolett.9b01127
9. Z. Liu, Y. Zeng, Q. Tang, A. Hu, K. Xiao, S. Zhang, W. Deng, B. Fan, Y. Zhu, X. Chen. Potassium vapor assisted preparation of highly graphitized hierarchical porous carbon for

high rate performance supercapacitors. J Power Sources. **361**, 70-79 (2017). https://doi.org/10.1016/j.jpowsour.2017.06.058

10. M. Chen, W. Wang, X. Liang, S. Gong, J. Liu, Q. Wang, S. Guo, H. Yang. Sulfur/oxygen codoped porous hard carbon microspheres for high-performance potassium-ion batteries. Advanced Energy Materials. **8**(19), 1800171 (2018). https://doi.org/10.1002/aenm.201800171
11. G. Ma, K. Huang, J.-S. Ma, Z. Ju, Z. Xing, Q.-c. Zhuang. Phosphorus and oxygen dual-doped graphene as superior anode material for room-temperature potassium-ion batteries. Journal of Materials Chemistry A. **5**(17), 7854-7861 (2017). https://doi.org/10.1039/C7TA01108C
12. Z. Ju, S. Zhang, Z. Xing, Q. Zhuang, Y. Qiang, Y. Qian. Direct synthesis of few-layer f-doped graphene foam and its lithium/potassium storage properties. ACS Appl Mater Interfaces. **8**(32), 20682-20690 (2016). https://doi.org/10.1021/acsami.6b04763
13. H. He, D. Huang, Y. Tang, Q. Wang, X. Ji, H. Wang, Z. Guo. Tuning nitrogen species in three-dimensional porous carbon via phosphorus doping for ultra-fast potassium storage. Nano Energy. **57**, 728-736 (2019). https://doi.org/https://doi.org/10.1016/j.nanoen.2019.01.009
14. X. Zhao, Y. Tang, C. Ni, J. Wang, A. Star, Y. Xu. Free-standing nitrogen-doped cup-stacked carbon nanotube mats for potassium-ion battery anodes. ACS Applied Energy Materials. **1**(4), 1703-1707 (2018). https://doi.org/10.1021/acsaem.8b00182
15. J. P. Perdew, K. Burke, M. Ernzerhof. Generalized gradient approximation made simple. Phys Rev Lett. **77**(18), 3865-3868 (1996). https://doi.org/10.1103/PhysRevLett.77.3865
16. B. Delley. From molecules to solids with the dmol3 approach. The Journal of Chemical Physics. **113**(18), 7756-7764 (2000). https://doi.org/10.1063/1.1316015
17. Y. Tian, Y.-j. Liu, J.-x. Zhao, Y.-h. Ding. High stability and superior catalytic reactivity of nitrogen-doped graphene supporting pt nanoparticles as a catalyst for the oxygen reduction reaction: A density functional theory study. RSC Advances. **5**(43), 34070-34077 (2015). https://doi.org/10.1039/C5RA02585K